Quantitative Distinction between Noble Metals Located in Mesopores from Those on the External Surface

Special Issue

Carolin Rieg,[a] Daniel Dittmann,[a] Zheng Li,[a] Robert Lawitzki,[b] Katrin Gugeler,[c] Sarah Maier,[a] Guido Schmitz,[b] Johannes Kästner,[c] Deven P. Estes,[a] and Michael Dyballa*[a]

Abstract: We compare three methods for quantitatively distinguishing the location of noble metal (NM) particles in mesopores from those found on the external support surface. MCM-41 and SBA-15 with NM located in mesopores or on the external surface were prepared and characterized by TEM. ^{31}P MAS NMR spectroscopy was used to quantify arylphosphines in complexes with NM. Phosphine/NM ratios drop from 2.0 to 0.2 when increasing the probe diameter from 1.08 to 1.54 nm. The reaction between NM and triphenylphosphine (TPP) within 3.0 nm MCM-41 pores takes due to confinement effects multiple weeks. In contrast, external NM react with TPP instantly. A promising method is filling the pores by using the pore volume impregnation technique with tetraethylorthosilicate (TEOS). TPP loading revealed that 66% of NMs are located on the external surface of MCM-41. The pore filling method can be used in association with any probe molecule, also for the quantification of acid sites.

Introduction

A key challenge for the design of heterogeneous catalysts is the accurate understanding of the catalytically active site and its accessibility. Especially for shape-selective heterogeneous catalysis in porous solids, the selectivity strongly depends on the spatial distribution of active sites. Therefore the location of Brønsted acid sites and noble metals (NM) is key to understanding of such catalysts. Typical approaches to investigate the Brønsted acid site distribution make use of probe molecules, where a spectroscopically detectable interaction between probe and active site occurs. Using probe molecules of different sizes gives information on the quantitative spatial distribution of the accessible sites.[1] Such approaches are commonly used for determining the spatial distribution and accessibility of Brønsted acid sites in systems containing micropores or containing a hierarchical micro-/mesopore system.[2]

The investigation of the spatial distribution of noble metals is more challenging. Detailed information on the state of the noble metals before, during, and after catalysis is gained by X-ray absorption spectroscopy.[3] Comparable information is gained from X-ray diffraction.[4] Measurements in sufficient accuracy for simulation, however, require high fluxes or long measurement times. Thus, time and cost considerations limit the use of 3-D measurements. Even if the location of sites is known, this does not confirm their accessibility for reactant molecules. An alternative approach is the use of high-resolution microscopy. Jiao and Regalbuto investigated palladium nanoparticles supported on SBA-15 with high resolution scanning transmission electron microscopy (STEM).[5] Focusing on a sample area and tilting the sample by $\pm 20°$ had no effect on particles within SBA-15, while particles located at the edges lost focus. Weyland et al.[6] located Pd_6Ru_6 nanoparticles within MCM-41 pores by the use of three-dimensional electron microscopy. Using standard high-resolution transmission electron microscopy (TEM) and high-resolution scanning transmission electron microscopy (STEM), only two-dimensional location of noble metals is possible in a spatial resolution of around 1 nm, by comparing the particle sized with the pore diameters.[7] A disadvantage of such microscopy methods is that only specific areas can be investigated while a quantitative averaging over the whole sample remains difficult.

There is no easily applicable standard method for quantitatively determining the spatial distribution of noble metals. In particular, distinguishing between locations inside mesopores and on the external surface is challenging. It is our intention to close this gap. A novel approach for the quantitative determination of noble metal loadings is the use of arylphosphines of varying diameter. These probe molecules have been used to complex noble metals and acid sites making use of the 100%

[a] C. Rieg, D. Dittmann, Z. Li, S. Maier, Prof. D. P. Estes, Dr. M. Dyballa
Institute of Technical Chemistry
University of Stuttgart
Pfaffenwaldring 55, 70569 Stuttgart (Germany)
E-mail: michael.dyballa@itc.uni-stuttgart.de
[b] Dr. R. Lawitzki, Prof. G. Schmitz
Institute of Materials Science
University of Stuttgart
Heisenbergstraße 3, 70569 Stuttgart (Germany)
[c] K. Gugeler, Prof. J. Kästner
Institute for Theoretical Chemistry
University of Stuttgart
Pfaffenwaldring 55, 70569 Stuttgart (Germany)

Supporting information for this article is available on the WWW under https://doi.org/10.1002/chem.202102076

Part of a Special Issue on Contemporary Challenges in Catalysis.

abundant $I=1/2$ ^{31}P nucleus and the quantification of the complex forming between NM and phosphine by NMR spectroscopy.[8,9] A recently elaborated strategy to distinguish noble metals located on external surfaces from noble metals in micropores is the application of phosphine probes of different size, namely triphenylphosphine (TPP) compared with tri(4-methoxy)phenylphosphine (TMPP).[9] Triphenylphosphine can similarly be used to detect Brønsted acid sites.[10]

Here, we synthesize and characterize materials like mesoporous MCM-41 and SBA-15 with and without noble metal deposits. We compare three methods for distinguishing noble metals located in mesopores from those located on the external surface. Firstly, we use arylphosphine probe molecules of increasing size, the classical approach. Secondly, we show how the confinement of noble metals in mesopores slows down the complex formation with TPP. Finally, we elaborate a selective pore filling approach followed by complex formation with TPP. This results in a quantitative density of platinum noble metals deposited on the external surface. With this toolkit at our disposal, the quantitative location of active sites in micropores, mesopores, or on the external surface is possible. Most interestingly, the pore filling method is not restricted to noble metals, but can be used with any probe molecule, also with such for the quantification of Brønsted acid sites. Thus, one can for the first time quantitatively distinguish sites located on the external surface and from those within mesopores.

Results and Discussion

DFT calculations on the probe molecule size

With a growing library of arylphosphine probes, we need an accurate determination of the sizes of these potential ligands. In a previous report, these sized were estimated.[9] Herein, the estimations from the work of Hjortkjaer et al.[11] were replaced by DFT-calculations on the diameter of the molecules. The Conformer-Rotamer Ensemble Sampling Tool (CREST) was applied for conformer search, followed by DFT optimization at the B3LYP-D3 level, and the smallest diameters found for the molecules are presented in Table 1.[12] The variation in the diameter between the conformers is in a range of 0.02 nm for triphenylphosphine (TPP) and up to around 0.3 nm for tri(4-phenoxy)phenylphosphine (TPPP). The ligand sizes were approximated from static visualization of the molecules. However, each ligand's dynamic mobility may allow it to pass a pore that is slightly smaller than the diameters shown in Table 1.[13] For the smallest ligand, TPP, a minimum diameter of 1.08 nm was found, which is significantly larger than the 0.72 nm calculated by Hjortkjaer et al.[11] In contrast, Okumura et al.[13] described the size of TPP as 1.0 nm, which is significantly closer to the calculated values. Furthermore, we estimated a minimum diameter of 0.91 nm for the tri(4-methoxy)phenylphosphine (TMPP) molecule, whereas a diameter of 1.30 nm, was calculated by DFT. For the largest ligand (TPPP), the diameter calculated by DFT is 1.54 nm. A graphical representation of the TPP, TMPP and TPPP ligands using van der Waals radii can be found in Figure S1 in the Supporting Information.

Table 1. The DFT-calculated diameter representing the minimum diameter of a cylindrical pore through which the respective phosphine fits.

Probe molecule	diameter (nm)
TPP	1.08
TMPP	1.30
TPPP	1.54

Physicochemical characterization of the materials

We next investigate the properties of the parent materials by standard characterization techniques. Chemical analysis by ICP-OES shows that parent materials, silica Aerosil® A200 and mesoporous materials MCM-41 and SBA-15 are pure and contain nearly exclusively silicon atoms, but no aluminum impurity (Si/Al >1000). Other properties of A200 silica were previously described.[8] X-ray diffraction (XRD) patterns of purely siliceous MCM-41, and SBA-15 can be found in Figure S2 and S3 in the Supporting Information. Observation of the typical reflections of mesoporous MCM-41 and SBA-15 indicate that the synthesis was successful and that the pore system is intact after removing the template.[14,15] The MCM-41 shows one clear reflection from the (100) plane and two weaker ones from the (110) and (200) planes. SBA-15 shows a strong reflection from the (100) diffraction plane, and two from the (110) and (200) planes. The powder patterns do not change in intensity or reflection location after noble metal deposition, oxidation, and reduction, indicating a stable pore system. SEM pictures of the mesoporous parent materials are found in the Supporting Information, in Figure S4 for MCM-41 and in Figure S5 for SBA-15. The parent MCM-41 material particle diameters range from 0.5 to 2 μm, while parent SBA-15 material particles diameters range from 5 to 20 μm. In pictures of the SBA-15 material, the hexagonal growth symmetry is clearly reflected by the particles' SEM pictures. N_2-physisorption data of the parent materials can be found in Table 2. The mesoporous material MCM-41 exhibits a BET surface area of 860 m^2/g, with a mesopore diameter of 3.0 nm and a mesopore volume of 0.40 cm^3/g, in good agreement with literature data.[15] SBA-15 exhibits a BET surface area of 730 m^2/g, with a mesopore diameter of 6.5 nm and a

Table 2. N_2 physisorption data of supports A200, MCM-41, SBA-15 and the solid acid amorphous silica-alumina (ASA).

Sample	BET surface [m^2/g]	Pore diameter [nm][a]	Micropore volume [cm^3/g]	Mesopore volume [cm^3/g][b]
A200	180	4.5	–	0.60
MCM-41	860	3.0	0.17	0.40
SBA-15	730	6.5	0.08	0.79
ASA	350	~6[c]	0.01	n.d.[c]

[a] BJH method from the adsorption branch [b] subtracting micropore volume from the total pore volume at $p/p_0=0.99$ [c] amorphous without defined pores, diameter from adsorption branch

mesopore volume of 0.79 cm^3/g, also in good agreement with literature data.[9]

Aluminum-containing amorphous silica-alumina (ASA) with a Si/Al ratio of 3.0 was characterized previously.[10] The amorphous ASA particles appear in diameters of 5–10 μm size (see Figure S6 in the Supporting Information). It has a BET surface area of 350 m^2/g but no mesopores and a negligible micropore volume. These properties fit the literature on comparable systems.[16] The ^{27}Al MAS NMR spectrum of ASA show peaks at chemical shifts of $\delta_{27Al} = 56$, 27, and 4 ppm that can be assigned to aluminum in tetrahedral, pentahedral, and octahedral coordination, respectively. The acid site density of the material was determined to 0.35 mmol/g by quantitative loading with ammonia.[10] This material was used for protonation experiments with TPPP only and not used for introducing noble metals (NM).

Most herein described samples contain platinum (Pt) as the NM component. The deposition of Pt according to the standard procedure resulted in comparable loadings of samples between 0.7 and 1.6 wt% determined by ICP-OES (see Table 3). TEM pictures of 1.6Pt/A200 can be found in Figure S7 in the Supporting Information. The presence of nanoparticles could furthermore be proven by wide-angle XRD showing the typical reflections of platinum metal (see Figures S8 and S9 in the Supporting Information) with the (111), (200), and (220) planes located at 2θ values of 39.8°, 46.2°, and 67.5° degrees, respectively. This is in good agreement with literature.[7,17] H_2-chemisorption measurements were performed showed that all catalysts had a good dispersion of 62% and above. Thus, it is assured that the nanoparticles are finely distributed and enough binding sites for probe molecules exist. The dispersion of rhodium on silica A200 (around 100%) is very high, due to the herein assumed H/NM stoichiometry of 1:1 that overestimates the dispersion. Conclusively, a H/NM stoichiometry exceeding 1 is frequently reported in literature, for example Candy et al.[18], Drault et al.[19], and Bernal et al.[20] observed a H/NM stoichiometry of up to 4.5.

To prove that the noble metals nanoparticles are located inside the mesopores, we took TEM images of platinum loaded MCM-41 and SBA-15, visible in Figure 1. We verified the chemical composition of the black dots by EDX measurements. However, note that the images can only observe larger NM particles of multiple nanometer diameter instead of small atom clusters. This explains a certain discrepancy between impressions from TEM images and dispersions calculated from H_2-chemisorption measurements. In accordance with this, the TEM images of 1.6Pt/A200 show few NM particles of up to 10 nm diameter. Highly-distributed clusters of only a few atoms in diameter stay invisible and an assignment of the areas of higher contrast to such particles remains speculative. According to TEM, the parent MCM-41 has diameters of around 3 nm. From Figure 1 (top), Pt particle sizes of 2 nm to 3 nm can graphically be estimated for 1.0Pt/MCM-41_in. Few particles of larger size up to 4 nm are found. Conclusively, the nanoparticles are predominantly present inside the mesopores and to a lower extent on the external surface in good dispersion (62%). The material 0.7Pt/MCM-41_out in Figure 1 (middle) was impregnated with the noble metal salt solution before the calcination procedure, so the nanoparticles are expected on the external surface of the particles. Indeed, the TEM images show nanoparticles with diameters from 5 to 13 nm in Figure 1 (middle row). The deposition on the outer surface of MCM-41 also resulted in stronger agglomeration of some platinum, leading to "lines" of agglomerated NM (right picture). This is expected, as only the external surface area is available when the MCM-41 pores are blocked by the template. The visible particles are too large for the mesopores and located on the outer surface, as result of the applied surface-selective deposition method. In the

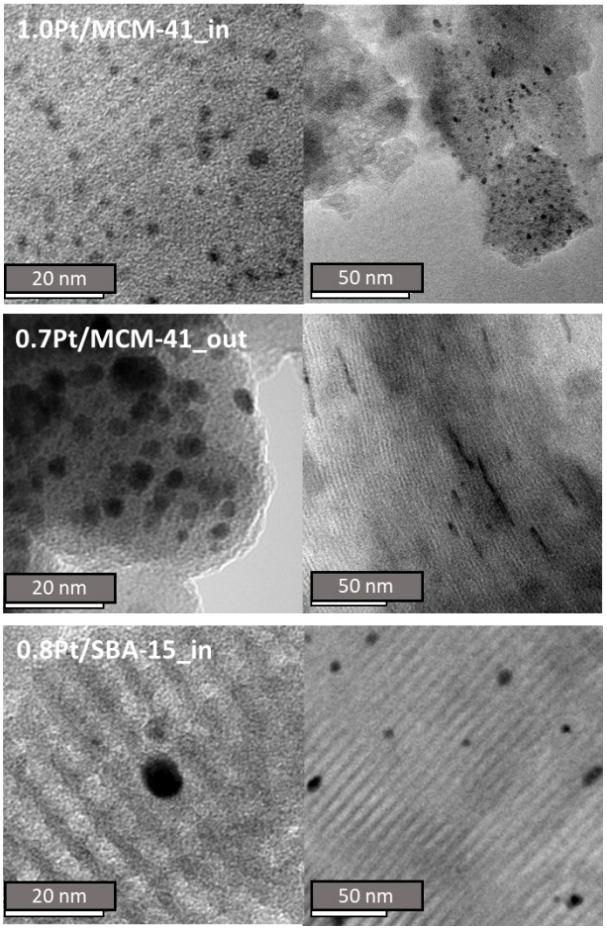

Figure 1. TEM images of material calcined after platinum deposition.

Table 3. Noble metal nanoparticle properties of samples under investigation.

Sample	Loading [wt.%][a]	Loading [μmol/g][a]	Dispersion [%][b]
1.6Pt/A200	1.6	80	73
0.9Rh/A200	0.9	87	101
1.1Pd/A200	1.1	103	79
1.0Pt/MCM41_in	1.0	51	62
0.7Pt/MCM41_out	0.7	38	84
0.8Pt/SBA15_in	0.8	41	91

[a] ICP-OES, accuracy ±10% [b] H_2-chemisorption

TEM-images of SBA-15 (bottom) material, the honeycomb structure and unidirectional pores of the hexagonal symmetry are clearly visible. The sample 0.8Pt/SBA-15_in was prepared like MCM-41_in by wet impregnation. The pore diameter of the parent material is 6.8 nm, according to TEM images. Thus, larger particles can form within SBA-15 compared to MCM-41. The platinum deposited on 0.8Pt/SBA-15_in forms particles of up to 6 nm located inside the pores and visible by TEM. Because wet impregnation was applied, some particles of up to 8 nm are too large for the mesopores and thus located on the external surface. Note that the successful deposition of noble metal particles on the external surface is limited to MCM-41 and was not possible for the selective deposition of platinum on the external surface of SBA-15. There the salt is able to enter the pores of template-containing SBA-15, resulting in highly dispersed NM particles.[21]

Method 1: Probes of increasing diameter: TPP, TMPP, and TPPP

A common way to quantitatively evaluate active site location is the spectroscopic quantification after loading with probe molecules of different diameter. For noble metals the use of phosphines enabled discrimination between particles located in micro- and mesopores.[9] Likewise, Brønsted acid sites in micropores were distinguished from those located on the external surface and in mesopores.[10] Here, we use TPPP (with a diameter of 1.54 nm) for distinguishing noble metals in mesopores from noble metals on the external surface of mesoporous materials. The solid-state ^{31}P MAS NMR spectra of TPPP treated at different temperatures and on various supports without NM as well as peak assignments are shown in Figures S10 and S11 and Table T1 in the Supporting Information.

A comparison of the three probe molecules TPP, TMPP, and TPPP binding to platinum loaded on A200 is found in Figure 2 and a summary of quantitative data on the binding is found in Table 4. We will first focus on the probe molecules TPP and TMPP. After loading our materials, we observe literature-known peaks of metal-phosphine complexes at a chemical shift around 35 ppm, and the peaks of bulk interactions and crystalline phase at $\delta_{31P} = -6$ and -9 ppm for TPP and at $\delta_{31P} = -10$ and -15 ppm for TMPP, respectively.[9] Table 4 enables the direct comparison of samples. The intensities of the broad low-field peaks lead to the numbers of complexed probe molecules summarized in Table 4, column 4 and the corresponding phosphine/NM ratios in Table 4, column 5. The intensity of the peaks of TPP and TMPP in complexes was evaluated by referring to an external standard, resulting in 161 or 134 μmol/g of complexed phosphines. This corresponds to phosphine/Pt ratios

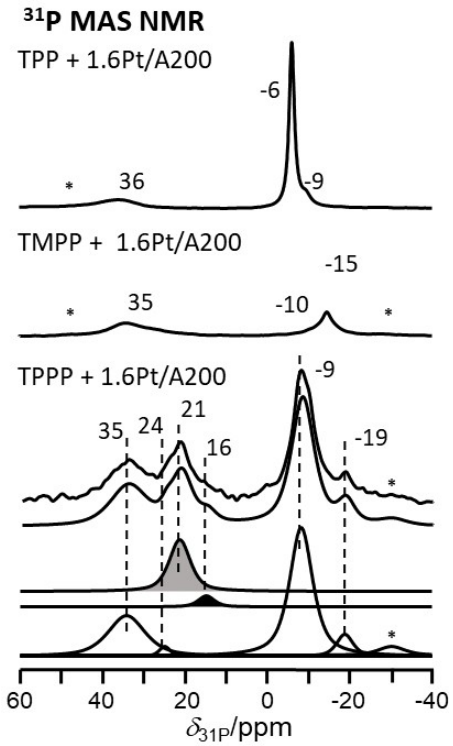

Figure 2. Metal binding probe molecules TPP, TMPP, and TPPP on 1.6Pt/A200 (intensities adjusted). For TPPP, we show (from top to bottom) original spectra and sum of fitted components, peaks indicating interaction with metal (grey) or surface (black), and peaks of bulk TPPP (white). Spinning sidebands are marked by asterisks (*).

Table 4. Phosphine probe molecules complexed with noble metals (NM) and phosphine/Pt ratios.

sample	platinum (Pt) loading in [μmol/g][a]	used phosphine probe molecule	complexed phosphine [μmol/g][b]	phosphine/Pt ratio
1.6Pt/A200	80	TPP	161	2.0
1.6Pt/A200	80	TMPP	134	1.7
1.6Pt/A200	80	TPPP	17	0.2
0.9Rh/A200	87	TPPP	4	<0.1
1.1Pd/A200	103	TPPP	–	–
1.0Pt/MCM41_in	51	TPP	92	1.8
1.0Pt/MCM41_in	51	TPPP	–	–
0.7Pt/MCM41_out	38	TPP	68	1.8
0.7Pt/MCM41_out	38	TPPP	–	–
0.8Pt/SBA15_in	41	TPP	120	2.9
0.8Pt/SBA15_in	41	TMPP	38	0.9
0.8Pt/SBA15_in	41	TPPP	14	0.3

[a] ICP-OES, accuracy ±10% [b] ^{31}P MAS NMR, accuracy ±10%

of 2.0 or 1.7, respectively (see Table 4). This is in good agreement with previous findings and the higher binding stoichiometry of TPP compared to TMPP can be explained by the smaller size of TPP molecules.[9] The increasing size of the phosphine ligands complicates the formation of a complex, as the phosphines become more and more sterically demanding.

Loading TPPP on the aforementioned 1.6Pt/A200 leads to peaks assigned to bulk TPPP located at a chemical shift of $\delta_{31P} =$ 35, 24, −9, and −19 ppm, respectively. A peak at 16 ppm occurs due to physiosorbed TPPP interacting with the surface of the silica materials. Another peak at 21 ppm occurs exclusively for TPPP in the presence of the NM and is thus assigned to a complex between phosphine and NM. The intensity of this peak corresponds to a phosphine loading between 15 and 19 μmol/g, leading to an average phosphine/NM ratio of 0.2. This is an order of magnitude smaller than the ratio determined for TPP or TMPP (see Table 4). Due to its size causing steric restrictions, TPPP struggles to form stable complexes with NM. This demonstrates the limitation of an approach relying on sterically demanding probe molecules for directly probing NM located inside and outside of mesoporous materials, as the probes get simply too big to form complexes in reasonable quantities. For comparison, platinum can form complexes with TPP or TMPP in a stoichiometry with phosphine/NM ratio up to 3.[9] TPPP was herein also checked for its ability to form a complex with rhodium and palladium deposited on A200 respectively, using samples that form complexes with TPP and TMPP.[9] Only very little complexation was observed with rhodium (see Figure S12 in the Supporting Information). We also loaded porous 1.0Pt/MCM-41_in and 0.7Pt/MCM-41_out with TPPP under optimized conditions. However, we could not find peaks at 21 ppm that indicate a binding between TPPP and platinum. A spectrum of TPPP loaded on 0.8Pt/SBA-15_in resulting in a phosphine/NM ratio of 0.3 can be found in Figure S13 in the Supporting Information. A higher stoichiometry on 0.8Pt/SBA-15_in is observed with TMPP (38 μmol/g), corresponding to a phosphine/Pt ratio of 0.9. The highest stoichiometry is observed with TPP (120 μmol/g), leading to a phosphine/Pt ratio of 2.9. Thus, the size of the probe molecule has a major impact on the ability of complexation inside pores. The bigger the probe, the smaller the phosphine/Pt ratio and likewise the sensitivity of the method. This represents a major disadvantage if it comes to the use of probe molecules so bulky that they cannot enter mesopores.

Method 2: Slower TPP complex formation under confinement

We next focused on the equilibration time required for the samples to reach a steady state. We describe another method indicative for the noble metals (NM) location. We previously observed that sometimes an equilibration (at RT under N_2) was necessary to maximize the intensity of the peak assigned to NM complexes.[9] Since MCM-41 has a smaller average pore diameter than SBA-15 (3.0 nm vs. 6.5 nm) and a complex with diameter of two TPP-molecules would exceed 2 nm, this might result in a slower complex formation within MCM-41 mesopores. A long equilibration time until a constant peak intensity is reached would thus be a sign of strong confinement of complexes. It would thereby indicate confined NM particles within pores. We started to investigate the complex formation of phosphines with NM located in mesopores of material 1.0Pt/MCM-41_in (see Figure 3). The intensity of the peak at 36 ppm, assigned to complexed phosphines, increases from an initial value of ~1 μmol/g directly after heat treatment to a stable, maximum value of 92 μmol/g after a total equilibration time of 8.5 weeks. The peak intensity remained constant afterwards. In between measurements, the sample was stored in closed rotors at RT under N_2 atmosphere. Note, that the initial value of 1 μmol/g is not representative for the quantity of external NM, despite the TPP being distributed under previously determined standard conditions.[8,9] Slight changes in this equilibration procedure, especially intensive mixing or multiple heat treatments, resulted in higher intitial values of up to 31 μmol/g instead of 1 μmol/g. However, the final value of 92 ± 2 μmol/g was reproduced after several weeks equilibration, which corresponds to a phosphine/Pt ratio of 1.8. In accordance with TEM images, we conclude from the lower initial y-intercept that only small amounts of NM are located on the external surface of 1.0Pt/MCM-41_in. However, their exact quantification remains challenging due to the mentioned influences of the preparation.

For a direct comparison to NM deposited on the outer surface of MCM-41, we investigated 0.7Pt/MCM-41_out. The platinum is located mainly on the outer surface of the material. We get directly after heating a constant intensity of 68 μmol/g associated with the peak located at 36 ppm, in a phosphine/Pt ratio of 1.8. Similar phosphine/Pt ratios of 1.0Pt/MCM-41_in and 0.7Pt/MCM-41_out indicate that formed complexes have the same stoichiometry on both materials. The immediate maximum value for 0.7Pt/MCM-41_out indicates good accessibility of NM on the external surface. To investigate the influence of a larger mesopore diameter on the complex formation equili-

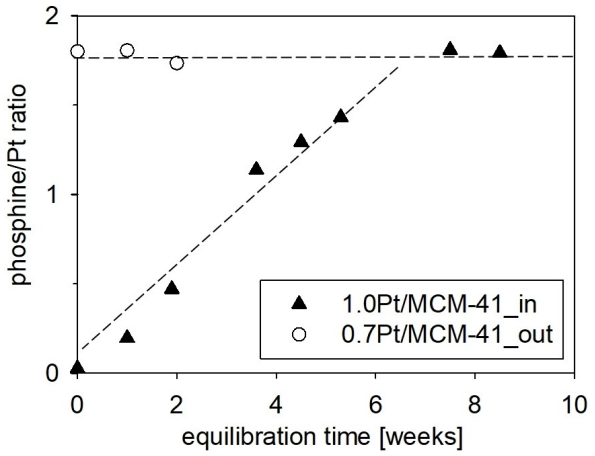

Figure 3. Phosphine/Pt ratios over time for TPP binding on 0.7Pt/MCM-41_out with NM deposited selectively on the external surface and 1.0Pt/MCM-41_in with NM deposited inside the pores. Both reach a ratio of 1.8, however, in significantly different time scales.

brium, we also loaded TPP on 0.8Pt/SBA-15_in. In accordance with previous results, we find constant phosphine/Pt ratios after 1 week equilibration time.[9] Subsequently we loaded 0.8Pt/SBA-15_in with the bigger probe TMPP but found no changes in the peak intensity of the 36 ppm peak over time. In steady state, 38 μmol/g phosphines bound with platinum, representing a phosphine/Pt ratio of 0.9 (see Figure S14 in the Supporting Information). Despite the bigger TMPP might have slower diffusion, it seems the ratio between probe and pore diameter affects the complex formation time stronger. Thus, the time dependence of complex formation indicates NM confined within pores, when pore diameter and probe molecule size fit to a certain extent. As distinguishing noble metals inside and outside mesopores by equilibration time is not a broadly applicable method, we present a strategy to probe the location of noble metal particles without pore diameter limitations in the following.

Method 3: Filling mesopores and TPP loading

In previous sections, we used the approach of varying probe size and complex formation time. Depending on the location of NM particles, larger phosphines as TPPP could not access them to form complexes. In contrast, TPP accessed all NM resulting in higher phosphine/NM ratios. Both are schematically visualized in Figure 4, top row. However, as shown previously, TPPP barely reacts with NM (in contrast to the smaller TPP). The resulting low phosphine/NM ratios render a quantitative interpretation imprecise. In this section, we aim to selectively cover NM located in pores. In a second step, we then use TPP to quantify the remaining uncovered, external NM.

We test three deposits in their applicability at filling the pores, as represented in Figure 4. First, we use the SBA-15 template, a P123 polymer, which diffuses into the pores.[22] It covers NM located within the pores so that only external NM will be accessible for TPP. Second, we apply acid-catalyzed saccharose polymerization to clog the pores with a denser inert material. And third, we pore-impregnate with tetraethylorthosilicate (TEOS) followed by subsequent calcination to SiO_2. TEOS, deposited by chemical liquid deposition, was previously used by Zheng et al.[23] for covering the external surface of zeolite ZSM-5. Here, pores are not completely filled, only their surfaces are covered. For application as quantitative method, we defined 3 criteria that have to be fulfilled:

1. Negative test. The deposits alone, without NM, do not lead to peaks in ^{31}P MAS NMR in the region 35 ± 10 ppm. We checked this on parent materials without NM.
2. The pore filling reagent does not inactivate the NM surface upon contact. A coincidental covering of NM or covering on purpose however cannot be excluded or is even desired. We checked this by a treatment on 1.6Pt/A200 and subsequent TPP loading.
3. Mesopores can be filled selectively so that i) only internal NM are covered and ii) external NM stay intact without leaching.

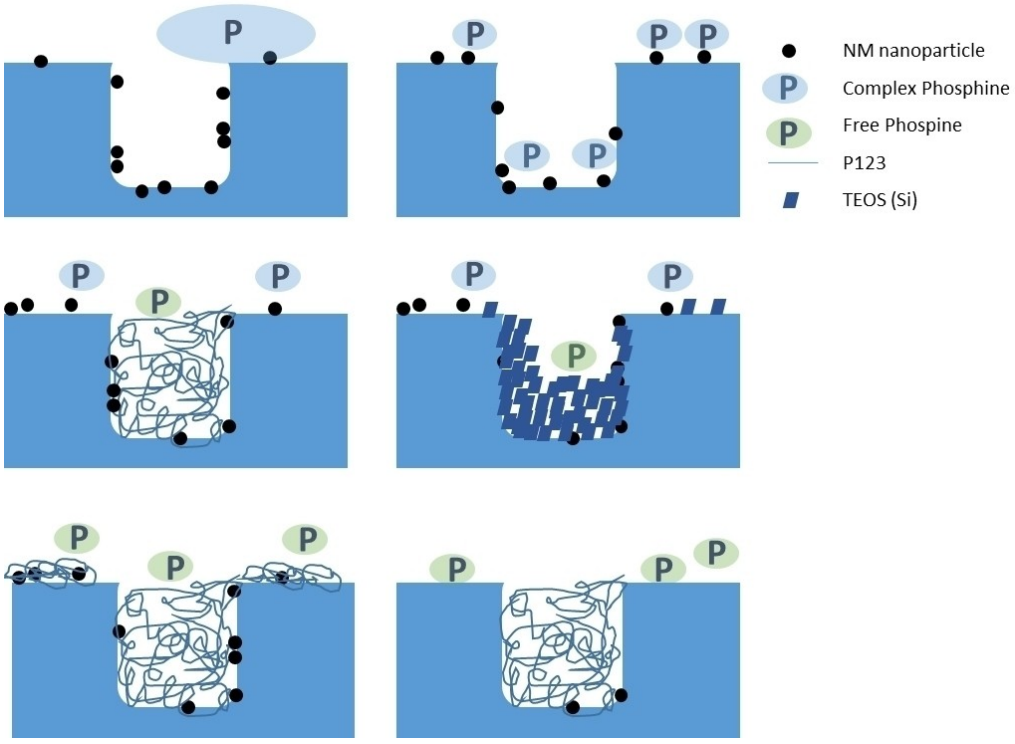

Figure 4. Schematic representation of the strategies followed within this contribution. First row: Two probes with different sizes, only the small one can enter (Method 1, 2). Middle row: Pore filling with P123/Saccharose and with TEOS (Method 3, successful). Bottom row: the NM cannot be reached by TPP if they are covered by a filler or removed by leaching (Method 3, with an unsuited filler).

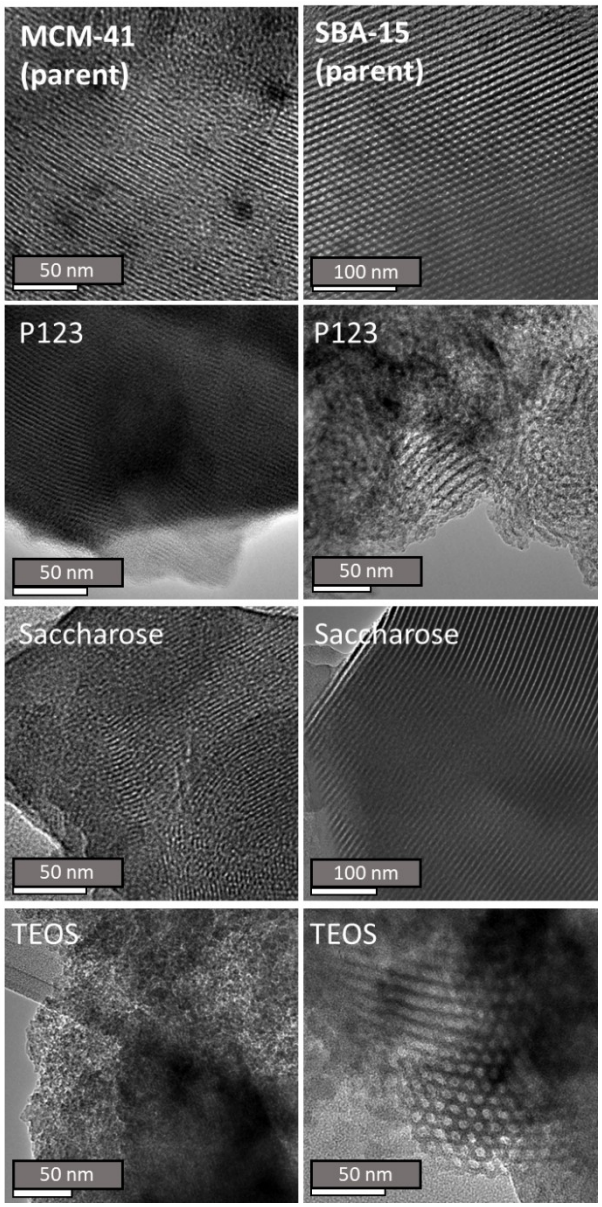

Figure 5. TEM images of MCM-41 (left column) and SBA-15 (right column) materials. The first row shows the parent materials, the second row the respective materials filled with P123, the third row filled with saccharose, and the bottom row filled with TEOS.

Table 5. N_2 physisorption data of filled MCM-41 and SBA-15 materials.

Sample; filler	BET surface [m^2/g]	Pore diameter [nm][a]	Micropore volume [cm^3/g]	Mesopore volume [cm^3/g][b]
MCM-41; P123	90	3.8	3.8	3.8
SBA-15; P123	690	5.7	5.7	5.7
MCM-41; Sach	10	4.1	4.1	4.1
SBA-15; Sach	110	3.2	3.2	3.2
MCM-41; TEOS	500	3.6	3.6	3.6
SBA-15; TEOS	660	7.1	7.1	7.1

[a] BJH method from the adsorption branch [b] subtracting micropore volume from the total pore volume at $p/p_0 = 0.99$

TEM images of filled parent materials taken with strong under focus for contrast improvement are presented in Figure 5. Density changes between free pore and pore wall lead to Fresnel fringes, resulting in a significant contrast between empty pores and pore walls visible in the pictures. If pores are filled, the contrast observed in the pictures under constant measurement conditions is decreased as the density difference between pore and pore wall decreases. N_2-physisorption measurements on MCM-41 and SBA-15 materials filled with P123, saccharose (Sach) and TEOS are found in Table 5. The filling with P123 leads to a reduced contrast between pore wall and pores, especially on the edges of the particles and at the pore mouths. The BET surface of MCM-41 decreases dramatically from 860 to 90 m^2/g (compare Table 2). For SBA-15 the contrast in TEM images is stronger and the BET decreased barely from 730 to 670 m^2/g, which in turn shows that the pores are not completely filled. As P123 is not stable under the herein applied reduction conditions, we reduced the NM prior to filling with P123. Spectra of materials filled with P123 and subsequently probed with TPP are found in Figure S15 in the Supporting Information. After loading the parent A200, we found only the peaks of TPP deposited on the A200 surface and of bulk TPP at $\delta_{31P} = -6$ and -9 ppm. Second, we tested 1.6Pt/A200 to prove intact NM on the surface, but found again no interaction with the NM. We conclude that either the P123 completely covered the NM or that it reacted with them. Also on 0.7Pt/MCM41_out no complex formation between TPP and NM could be observed and, likewise, a probing of 0.8Pt/SBA-15_in with TPP after P123 treatment was not successful. However, on 0.8Pt/SBA-15_in a weak and broad peak around 33 ppm (intensity would result in a phosphine/Pt ratio 0.1 to 0.2) built up after ~4 weeks equilibration time (all samples stored in closed rotors under dry N_2). We conclude that TPP is able to diffuse through the pores, as did the metal salts in previous reports, or that an undesired side-reaction occurs.[21] Thus, no quantification of NM by loading with TPP was possible and the method is not suitable for a selective detection of NM on external surfaces.

We searched for an inert filling agent that would resist the reduction conditions (3 h at 623 K in pure H_2-stream). We thus tested filling with saccharose and a subsequent calcination in air for this purpose. The samples were calcined before the treatment to distribute the PtO_2 and they were reduced in a final step directly before the TPP loading. Evaluating the TEM pictures in Figure 5 of parent filled with saccharose, however, reveals a strong contrast between pore walls and inner pore volume, compared with P123. This could be a sign for incomplete pore filling. However, pores are inaccessible as the BET surface area of MCM-41 and SBA-15 decreased to 10 respectively 110 m^2/g (see Tables 2 and 5). The ^{31}P MAS NMR spectra of saccharose-treated samples after subsequent loading with TPP are found in Figure S16 in the Supporting Information. Again, the initial test on A200 was negative, so the pore filling agent saccharose is not interacting with TPP. Second, we tested if nanoparticles are inhibited by the saccharose. Probing 1.6Pt/A200 with TPP gave no peak at ~35 ppm. Conclusively, the treatment with saccharose is not selective to the pores and/or it

is unclear if it covers the NM or leaches them. To exclude a coverage, we removed the saccharose deposited on the external surface. Therefore, we applied cautious rinsing with water before calcination of the saccharose. After subsequent reduction, this lead to a weak peak at ~38 ppm, which could be due to an interaction between TPP and NM. However, also by washing we could not observe any peaks of TPP interacting with NM on mesoporous materials (see Figure S16 in the Supporting Information). Thus, we could not develop a method based on saccharose for selective pore blocking without inactivating the NM.

As a last method, we performed the pore volume impregnation with TEOS and water followed by subsequent calcination. The samples were calcined before the treatment with TEOS/water, to distribute the PtO_2, and were reduced after the treatment with TEOS. Again, we started with a negative test evaluating the TPP state deposition on A200 material modified 3x with TEOS/water and subsequent reduction by ^{31}P MAS NMR (see Figure 6, top left). No peak at a chemical shift of δ_{31P} = 36 ppm appeared. Thus, the TEOS treatment does not lead to misleading peaks. Using the sample 1.6Pt/A200 and reacting it with TPP after TEOS filling did not result in a peak of complexed platinum. Again, we checked if the NM are inhibited for complex formation by contact with TEOS or if they are covered by the filling agent. We impregnated the material with TEOS/water and subsequently washed it with water prior to the calcination step. Now, we observed a weak peak at a chemical shift of δ_{31P} = 36 ppm. This peak is due to TPP interacting with metallic platinum in a phosphine/Pt ratio of 0.5 (see Table 6). The phosphine/NM ratio is significantly smaller than for unmodified 1.6Pt/A200 with 2.0 (see Table 4) and a similar phosphine/Pt ratio of 0.5 was reproduced after 3-fold TEOS/water treatment. Thus, the highly distributed PtO_2 was partially covered by TEOS and could therefore not be reduced in H_2 and thus not be detected by TPP (see Figure 4, middle and right).The uncovered nanoparticles stayed intact and were able to react with the phosphine. The filling agent TEOS thus fulfills criterion 2.

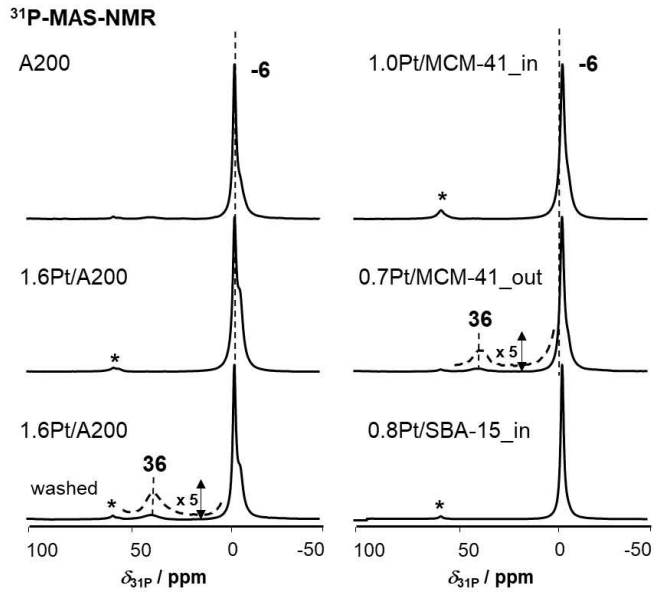

Figure 6. ^{31}P MAS NMR spectra of materials after treatment with TEOS, reduction, and subsequent TPP-loading. Spinning speed 10 kHz.

Table 6. Triphenylphosphine complexed with noble metals (NM) covered by TEOS and phosphine/Pt ratios.

Sample	platinum (Pt) loading in µmol/g [a]	complexed phosphine in µmol/g [b]	phosphine/Pt ratio
1.6Pt/A200	80	37	0.5
1.0Pt/MCM41_in	51	–	–
0.7Pt/MCM41_out	38	45	1.2
0.8Pt/SBA15_in	41	–	–

[a] ICP-OES, accuracy ±10% [b] ^{31}P MAS NMR, accuracy ±10%

We next investigate mesoporous materials. The TEOS/water mixture could be selectively deposited within mesopores using pore volume impregnation as requested by criterion 3. TEM images after modification of the parents shown in Figure 5 indicate a weak contrast between pore wall and inner pore. This is conclusive, as both parent and filling agent consist of amorphous SiO_2. From N_2-physisorption measurements and the only moderately decreased BET surface area of 500 respectively 660 m^2/g (see Tables 2 and 5), we conclude that pores were not completely blocked, as above reported for P123 and saccharose on MCM-41 and for saccharose on SBA-15. This is supported by the XRD patterns after filling with TEOS. SBA-15 reflections are maintained while the reflection intensities of MCM-41, having the smaller pore diameter, decreased after filling with TEOS (see Figures S17 and S18 in the Supporting Information). Thus, only the pore surface was covered by TEOS, as represented by the drawing in Figure 4, middle right. The first treatment was performed on 1.0Pt/MCM-41_in with Pt nanoparticles preferentially located within the mesopores (see Figure 6, right). No (quantifiable) peak at a chemical shift of δ_{31P} = 36 ppm is observed, thus the treatment with TEOS covered all nanoparticles and prevented them from a reaction with TPP. Due to the limited sensitivity of the method, a quantity of up to 4 µmol/g NM located on the outer surface of 1.0Pt/MCM-41_in cannot be excluded. This is in accordance with TEM images on NM distribution and the results from slow complex formation discussed in the previous section.

Secondly, we applied the method on the material 0.7Pt/MCM-41_out, with NM located preferentially on the external surface of the material. Here, a peak at δ_{31P} = 36 ppm appears which can be quantified to 45 µmol/g complexed TPP (see Table 6). As 68 µmol/g NM were detected without TEOS treatment (see Table 4), 23 µmol/g NM are located inside pores or could not be reached by the method. Thus, external sites are present in a phosphine/NM ratio of 1.2. Without filling the pores, a phosphine/NM ratio of 1.8 was reproducibly found for platinum NM particles located inside and outside MCM-41 pores (see Figure 3 and Table 4). Thus, 66% of the NM present on the pure 0.7Pt/MCM-41_out were directly detectable after TEOS treatments and must thus be accessiby located on the external surface. We tested if the pores could be filled to a greater

extent with SiO_2 by repeating the TEOS treatment up to 3 times. However, subsequent further TEOS treatments reduce these amounts (14 μmol/g NM detectable using 3 TEOS treatments). We thus recommend using only one TEOS treatment in order not to cover too many external surface sites. As some NM on 0.7Pt/MCM-41_out are located within pores or lost due to the TEOS treatment, 66% is a valuable result for the amount of NM still located on the external surface. The method can be transferred to other mesopore systems like 0.8Pt/SBA-15_in. This material did not show a (quantifiable) peak at 36 ppm and all nanoparticles within pores were covered. In accordance with TEM images and H_2-chemisorption we conclude that most NM are located within the respective mesopores. Furthermore, this is in line with the TPPP loadings, where we found complex formation on SBA-15 but not in the smaller pores of MCM-41, which also supports that most NM are inaccessibly located within the pores of the materials.

In conclusion, we tested if we could selectively fill the pores with inert material. Fragile P123 filled the pores to a high extent, but lead to no ^{31}P MAS NMR peaks that could clearly be assigned to complexes of TPP with NM. The saccharose polymerization showed a lower pore filling and tended to completely cover the surfaces or inactivate the NM. This problem could only partially be solved by washing. Pore volume impregnation with TEOS followed by calcination covered inner pore walls, while leaving the external surface accessible. NM located on the external surface stayed intact and reacted with phosphine, TPP. The extent of complex formation was quantified by ^{31}P MAS NMR and proved that at least 66% of NM located on sample 0.7Pt/MCM-41_out are located on the external surface (25.1 μmol/g platinum) and some were covered by TEOS deposition inside the pores (12.9 μmol/g). Note that TPP can also be used for the quantification of Brønsted acid sites.[10] The herein presented approach can thus easily be transferred for determining the spatial distribution of Brønsted acid sites, within mesopores or on the external surface.

Conclusion

In this contribution we aimed to quantitatively distinguish noble metal (NM) particles located on the external surface from NM located within mesopores of MCM-41 and SBA-15. The synthesis of MCM-41 with NM deposited to a high extent on the external surface was possible using template-containing mesoporous material, whereas this approach turned out impossible for SBA-15. The location of NM was checked by TEM and a sufficient dispersion was assured using H_2-chemisorption. We applied DFT-calculations to calculate the sizes of the probe molecules TPP, TMPP, and TPPP being 1.08, 1.30, and 1.54 nm, respectively. Then, we compared three different methods for this purpose. First, the complex formation with phosphines, namely triphenylphosphine (TPP), tri(4-methoxy) phenylphosphine (TMPP), and tri(4-phenoxy)phenylphosphine (TPPP) followed by quantification of ^{31}P MAS NMR peaks was performed. It turned out the phosphines have a different tendency to form complexes with NM: The smaller the probe, the higher the phosphine/NM ratio of the resulting complexes. For example, only 17 μmol/g of voluminous TPPP reacted with NM whereas on the same sample 161 μmol/g of the smaller TPP reacted with NM, leading to phosphine/NM ratios of 0.2 and 2.0, respectively. A similar picture was observed for NM within porous materials. In contrast to use of platinum, only few TPPP molecules bound to the noble metals rhodium and palladium deposited on A200. TPP was the most sensitive probe for detecting NM. If the NM was located within the 3.0 nm pores of MCM-41, complex formation with TPP took multiple weeks. Thus, a slow complex formation indicates that NM are confined within the pores and only minor amounts are present on the external surface. The maximum phosphine/NM ratio was achieved instantly after loading, if NM were located on the external surface of MCM-41. The final phosphine/NM ratio was equal for both NM locations, indicating that similar complexes form independent of NM location. Finally, we filled the pores with inert material and used TPP to quantify the NM located on the external surface. We could show that the rather instable P123 did not allow a quantifiable reaction of NM with TPP. Using the filling agent saccharose, we were able to reduce our NM particles in H_2 after filling the pores. However, saccharose was not selectively deposited within pores and covered also NM particles located on the external surface. A pore volume impregnation with tetraethylorthosilicate (TEOS) and water finally resulted in a sufficiently selective coverage of the inner pore walls rather than a complete pore blocking or covering of the external surface. The method prevents the occurrence of misleading peaks. If NM are confined within pores of MCM-41 and SBA-15, they cannot be detected by TPP after the pore filling with TEOS. In contrast, they are easily detected if deposited on the external surface of MCM-41 in a quantity of at least 66% of the total NM content. Using this procedure one can distinguish noble metals, and likewise Brønsted acid sites, within mesopores and on the external surface quantitatively in reasonable accuracy.

Experimental section

Synthesis procedures

Amorphous silica-alumina (ASA) was purchased from Saint-Gobain and calcined at 823 K for 5 h (if not stated otherwise: heating rate 1 K/min) prior to use. It was described previously and not used for noble metal (NM) exchange.[10] Commercial silica Aerosil® A200 (Evonik Industries, Germany) was calcined for 12 h at 823 K in synthetic air prior to use. The mesoporous SBA-15, having a specific surface area of 901 m^2/g and mesopore diameters between 6 and 7 nm, was synthesized as described by Zhao et al.[14] Briefly, 6 g of the surfactant Pluronic® P123 were dissolved in 192 mL water and 30 mL hydrochloric acid (37%) was added, followed by stirring for 1 h. The precursor tetraethylorthosilicat (13.2 g) was added slowly, followed by another stirring for 10 minutes. The batch of molar composition $1TEOS:0.016P123:4.7HCl:170H_2O$ was heated to 313 K and stirred for 24 h. A hydrothermal treatment was conducted in a 130 mL autoclave at 373 K for 24 h, the mixture was filtered, washed, and dried at 353 K for 12 h. To remove the template, the as-synthesized SBA-15 was heated at 2 K/min up

to 823 K and calcined in synthetic air flow for 5 h. The mesoporous MCM-41 was synthesized as described by Kumar et al.[24] Briefly, 2.4 g of the template cetyltrimethylammonium bromide (Sigma-Aldrich) was dissolved in 120 mL deionized water and stirred for 1 h. 10 mL ammonium hydroxide (pH ~ 10) were added dropwise, and after 10 minutes stirring 10 mL tetraethylorthosilicate (TEOS) was added. The material was washed after 20 h with water and dried at 363 K and calcined at 823 K for 5 h.

The loading of silica A200 with noble metal (NM) salts was carried out by strong electrostatic adsorption, stirring 5 g in 100 mL of demineralized water at 313 K for 2 h and subsequent addition of 1 M aqueous solution of ammonia until the pH-value of the solution reached 10. Then, an aqueous solution with calculated amounts of $[Pt(NH_3)_4]Cl_2{\cdot}xH_2O$ (ChemPur), $[Pd(NH_3)_4]Cl_2{\cdot}xH_2O$ (ChemPur), $RhCl_3{\cdot}x\ H_2O$ or $RuCl_3{\cdot}x\ H_2O$ was added dropwise. The solution was stirred at 313 K for another 18 h. Finally, the resulting solid was collected by filtration, washed with 1.5 L demineralized water, and dried at 353 K for 12 h. For both mesoporous parents (MCM-41 and SBA-15) the wetness impregnation technique was applied. Calculated amounts of the noble metal salts were dissolved in deionized water ($\beta = 5$ g/L) and added dropwise to the calculated amounts of mesoporous material. The water was then fully removed with reduced pressure and the obtained material was dried at 353 K for 12 h. After impregnation, all noble metal-containing samples were calcined in synthetic air (970 mL/min) at a rate of 0.5 K/min up to 573 K which was kept for 3 h in order to remove the volatile noble metal precursor components. The reduction was performed by heating the samples in pure H_2-stream (100 mL/min) at 623 K for 3 h (2 K/min heating rate). The samples were cooled down to room temperature over ca. 1 h, subsequently transferred into glass tubes inside a glove box under nitrogen atmosphere, evacuated at 298 K ($p < 10^{-2}$ Pa) for 12 h, and stored in sealed glass tubes until used. This resulted in the samples 1.6Pt/A200, 1.0Pt/MCM41_in, and 0.8Pt/SBA15_in, respectively. To obtain MCM-41 material with noble metals selectively deposited on the external surface, the template-containing parent material was impregnated with the noble metal salt solution before the calcination procedure. A subsequent reduction in H_2 as described above was performed prior to use of the material and lead to the sample 0.7Pt/MCM41_out.

Triphenylphosphine (TPP) and tri(4-methoxy)phenylphosphine (TMPP) were purchased from Sigma-Aldrich. Tri(4-phenoxy) phenylphosphine (TPPP) was synthesized according to a procedure by Davies et al.[25] that was modified by Saitoh et al.[26] All chemicals were purchased, if not stated otherwise, by Sigma-Aldrich. Briefly, 4-phenoxyphenylmagnesium bromide (3 equiv.) reacts with PCl_3 (1 equiv.) to TPPP (1 equiv.). The Grignard reagent was prepared by initially activating magnesium ($m = 7.45$ g, $n = 0.31$ mmol) in diethyl ether ($V = 20$ mL) under argon atmosphere by treatment with a small amount of iodine crystals at 298 K prior to use until the solution was colorless. Subsequently, 4-bromodiphenylether ($V = 10$ mL, $n = 0.057$ mol) was added dropwise and the resulting solution stirred for 18 h under reflux at 313 K. After cooling to room temperature, solid residues were removed by filtration. The 4-phenoxyphenylmagnesium bromide in diethyl ether was cooled to −78 °C with a dry ice/acetone bath and diluted with diethyl ether ($V = 10$ mL). PCl_3 ($V = 1.25$ mL, $n = 0.0143$ mol) was then added dropwise resulting in the precipitation of a yellow solid (reaction time). The solution was filtered under argon and the volume of the filtrate reduced by evaporation until solid began forming. Cooling at 253 K for 2 days resulted in the formation of yellow crystals that dissolved in ethanol under soft heating. After another 2 days another solid formed that was separated and dried for 2 h. It was washed with n-pentane and dried again in vacuo for 20 h. The resulting white-yellow TPPP powder was characterized via ^1H and ^{31}P NMR spectroscopy (400 MHz, *d*-acetone, barely soluble) showing chemical shifts $\delta_{1H} = 7.3$–6.9 ppm (multiple peaks, m) and $\delta_{31P} = -9$ ppm (s) (see Figure S19 in the Supporting Information (Supporting Information)). The melting point of 376 K agrees with the literature value of 384 K.[21]

Calculations and simulations

The size of TPPP was estimated with the software Avogadro by using unmodified structures from the PubChem database.[27] They were corrected using a factor derived from the density of triphenylphosphine at 373 K by Hjortkjaer et al.[11] A spherical geometry was assumed, as described previously.[9] For getting a reliable value for the ligand sizes, they were also calculated using density functional theory (DFT) and the semi-empirical GFN2-xTB method.[28] All DFT calculations were performed in Turbomole V7.1 in Chemshell via DL-FIND.[29] The initial ligand structures were pre-optimized using the GFN2-xTB method. Subsequent use of CREST resulted in various conformers within an energy range of 4 kJ/mol.[12] For the relevant conformers, optimizations were performed at the B3LYP-D3(BJ)/def2-SVP level.[30] From the optimized conformer structures, the ligand sizes were determined as the smallest diameter of a cylinder through which the rigid ligand would fit. Each atom is delimited by its van-der-Waals radius. The analysis was performed visually in VMD.[31]

Pore filling

In section 3.5 we explored the selective filling of mesopores using various materials. For some samples the pores were filled with P123 (Sigma Aldrich) similar to a procedure from literature.[22] Briefly, 1 g reduced material and 4 g Pluronic 123 were solved in 15 mL dried ethanol and stirred for 48 h in N_2-atmosphere. Then, the solvent was removed by centrifugation (10000 rpm, 10 min), the residue was dried in vacuum, and sealed air-tight, followed by the standard phosphine loading procedure. No subsequent reduction in H_2 was performed after pore filling. For some samples the pores were filled with D(+)-saccharose (Carl Roth GmbH & Co KG) and subjected to a polymerization procedure as described in literature.[32] Briefly, saccharose (0.89 g) was dissolved in water (~6 mL), and the catalyst material (0.67 g) was added. After stirring for 30 minutes oxalic acid (0.6 g) (Merck KGaA) was added, and the mixture was stirred for 24 h at room temperature. The next step was calcination in synthetic air (970 mL/min) for 5 h at 373 K, heating to 433 K in 5 h, and keep it at 433 K for 5 h. The impregnation and calcination procedure was repeated. Then, the materials were reduced, followed by the standard phosphine loading procedure. One sample was washed with 0.5 l demineralized water after stirring 30 minutes in oxalic acid, in order to remove surface deposits of saccharose. The next step was calcination in synthetic air (970 mL/min) for 5 h at pre-heated 373 K, heating to 433 K in 5 h, and keep it for 5 h. A subsequent reduction in H_2 as described above was performed and followed by the standard phosphine loading procedure.

In order to selectively deposit the TEOS within the pores, we conducted a pore volume impregnation followed by a calcination step. In one step, the pore volume determined by N_2-physisorption was thereby filled with a 1:4 stoichiometric

mixture of TEOS and water. The subsequent calcination was performed in synthetic air (970 mL/min) by heating in 6 h to 573 K (0.8 K/min), maintaining the temperature for 10 h, cooling to 423 K and keep it in N_2 atmosphere for another 3 h. A subsequent reduction in H_2 as described above was performed prior to use and followed by the standard phosphine loading procedure.

Characterization

X-ray diffraction was conducted on a Bruker D8 diffractometer with CuKα radiation ($\lambda = 1.5418$ Å), for mesoporous materials in a 2θ range of 0.5–5.0° and for analyzing the deposited noble metals in a 2θ range of 2–80°. The chemical composition and the noble metal content of the samples was determined by ICP-OES using an IRIS Advantage instrument. The samples were digested in HF and aqua regia prior to measurements. Adsorption and desorption isotherms of nitrogen were measured at 77 K on a Quantachrome Autosorb 3B instrument. Before the measurement, the samples were outgassed for 16 h at 623 K. Mesopore volumes were calculated from the total pore volume at $p/p_{0=}0.99$ and the micropore volume according to the V-t method (deBoer). The surface area was obtained applying the BET method. The noble metal dispersion was investigated by chemisorption of hydrogen using a Quantachrome Autosorb 1-C and assuming a 1:1 stoichiometry of H atom per noble metal atom. Scanning electron micrographs (SEM) were taken on a VEGA 3 instrument from TESCAN AG. Transmission electron micrographs (TEM) were obtained with a Philipps FEG CM200 operated at 200 kV and equipped with an EDX detector. Imaging in bright and dark field mode was applied and images were taken with small under-focus to contrast the pore structure. For TEM investigation, the materials were grinded with a pestle and suspended in ethanol. The suspension was then pipetted on a copper TEM grid with a lacey carbon film (Plano S166-4).

The loading with triphenylphosphine (TPP), tri(*p*-methoxyphenyl)phosphine (TMPP), (both Sigma-Aldrich) or tri(4-phenoxy)phenylphosphine (TPPP) was performed in a glove box purged with N_2 as described before.[8,9]. Briefly, air-tight glass vessels were weighted and dehydrated material for probing was added in a quantity up to 100 mg, depending on the desired ratio between probe molecule and material. Then the probe, TPP, TMPP (1–10 mg of respective probes), or TPPP (5–15 mg) was added as solid. The correct amount was controlled by weighting. The solids were mixed mechanically and filled into a 4-mm rotor, closed with an air-tight Torlon-cap with gas-tight O-ring. The rotor was again placed in a tight glass vessel and heated under N_2-atmosphere up to 20 h. The loading temperature depended on the probe molecules melting point and was 363 K for TPP, 393 K for TMPP, and 333 K for TPPP, if not stated otherwise. After the heat treatment, the materials were equilibrated up to multiple weeks under N_2 at room temperature, until a steady state was reached. ^{31}P MAS NMR measurements were carried out on a Bruker Avance III 400WB spectrometer at the resonance frequency of 161.9 MHz using a 4 mm MAS NMR probe with a sample spinning rate of 10 kHz. Spectra were recorded upon $\pi/2$ single-pulse excitation, high-power proton decoupling (HPDEC), and repetition times of 20 to 240 s for excluding saturation. Quantitative ^{31}P MAS NMR studies were performed by comparing the peak intensities of the samples under study with that of hydrated zeolite VPI-5 that was used as external intensity standard. Spectra were simulated using the software programs Bruker Top Spin and DMFIT.[33]

Acknowledgements

We thank Ann-Katrin Beurer, Dorothea Häussermann, and Heike Fingerle (all University of Stuttgart) for nitrogen adsorption studies and ICP-OES measurements. Also, we thank Hang Liu and Dorothea Häussermann for SEM measurements. MD thanks the Max-Buchner-Forschungsstiftung for their support. We gratefully acknowledge funding by the Deutsche Forschungsgemeinschaft (DFG, German Research Foundation) under project number 358283783, SFB 1333. Open Access funding enabled and organized by Projekt DEAL.

Conflict of Interest

The authors declare no conflict of interest.

Keywords: external surfaces · mesoporous materials · platinum, solid-state NMR spectroscopy · surface chemistry

[1] Y. Jiang, J. Huang, W. Dai, M. Hunger, *Solid State Nucl. Magn. Reson.* **2011**, *39*,116–14.
[2] a) M. Dyballa, D. K. Pappas, E. Borfecchia, P. Beato, U. Olsbye, K. P. Lillerud, B. Arstad, S. Svelle, *Microporous Mesoporous Mater.* **2018**, *265*, 112–122; b) Z. Li, M. Benz, C. Rieg, D. Dittmann, A.-K. Beurer, D. Häussermann, B. Arstad, M. Dyballa, *Mater. Chem. Front.* **2021**, *5*, 4254–4271; c) S.-P. Sheu, H. G. Karge, R. Schlögl, *J. Catal.* **1997**, *168*, 278–291; d) F. Thibault-Starzyk, I. Stan, S. Abelló, A. Bonilla, K. Thomas, C. Fernandez, J.-P. Gilson, J. Pérez-Ramírez, *J. Catal.* **2009**, *264*, 11–14.
[3] a) S. Bordiga, E. Groppo, G. Agostini, J. A. van Bokhoven, C. Lamberti, *Chem. Rev.* **2013**, *113*, 1736–1850; b) Y. Iwasawa in *XAFS Techniques for Catalysts, Nanomaterials, and Surfaces* (Eds.: Y. Iwasawa, K. Asakura, M. Tada), Springer International Publishing Switzerland, Basel, **2017**, p. 1.
[4] R. Schlögl, *Adv. Catal.* **2009**, *52*, 273–338.
[5] L. Jiao, J. R. Regalbuto, *J. Catal.* **2008**, *260*, 342–350.
[6] M. Weyland, P. A. Midgley, J. M. Thomas, *J. Phys. Chem. B* **2001**, *105*, 7882–7886.
[7] H. Wang, C. Liu, *Appl. Catal. B* **2011**, *106*, 672–680.
[8] M. Dyballa, C. Rieg, D. Dittmann, Z. Li, M. Buchmeiser, B. Plietker, M. Hunger, *Microporous Mesoporous Mater.* **2020**, *293*, p. 109778.
[9] C. Rieg, D. Dittmann, Z. Li, A. Kurtz, I. Lorenz, D. P. Estes, M. Buchmeiser, M. Dyballa, M. Hunger, *Microporous Mesoporous Mater.* **2021**, *310*, p. 110594.
[10] C. Rieg, Z. Li, A. Kurtz, M. Schmidt, D. Dittmann, M. Benz, M. Dyballa, *J. Phys. Chem. C* **2021**, *125*, 515–525.
[11] J. Hjortkjaer, Scurrell, M. S. P. Simonsen, H. Svendsen, *J. Mol. Catal.* **1981**, *12*, 179–195.
[12] P. Pracht, F. Bohle, S. Grimme, *Phys. Chem. Chem. Phys.* **2020**, *22*, 7169–7192.
[13] K. Okumura, M. Nakanishi, H. Takaba, *Microporous Mesoporous Mater.* **2017**, *241*, 400–408.
[14] D. Zhao, J. Sun, Q. Li, G. D. Stucky, *Chem. Mater.* **2000**, *12*, 275–279.
[15] V. Meynen, P. Cool, E. F. Vansant, *Microporous Mesoporous Mater.* **2009**, *125*, 170–223.
[16] B. Hu, I. D. Gay, *J. Phys. Chem. B* **2001**, *105*, 217–219.
[17] H. A. Huy, T. van Man, H. T. Tai, H. T. T. Van, *J. Sci. Technol.* **2016**, *54*, 472–482.
[18] J. P. Candy, A. Mansour, O. A. Ferretti, G. Mabilon, J. P. Bournonville, J. M. Basset, G. Martino, *J. Catal.* **1988**, *112*, 201–209.
[19] F. Drault, C. Comminges, F. Can, L. Pirault-Roy, F. Epron, A. Le Valant, *Materials* **2018**, *11*.
[20] S. Bernal, *J. Catal.* **1992**, *137*, 1–11.
[21] Y. Yin, Z.-F. Yang, Z.-H. Wen, A.-H. Yuan, X.-Q. Liu, Z.-Z. Zhang, H. Zhou, *Sci. Rep.* **2017**, *7*, 4509.
[22] F. Ziegler, J. Teske, I. Elser, M. Dyballa, W. Frey, H. Kraus, N. Hansen, J. Rybka, U. Tallarek, M. Buchmeiser, *J. Am. Chem. Soc.* **2019**, *141*, 19014–19022.

[23] S. Zheng, H. R. Heydenrych, A. Jentys, J. A. Lercher, *J. Phys. Chem. B* **2002**, *106*, 9552–9558.
[24] D. Kumar, K. Schumacher, C. Du Fresne von Hohenesche, M. Grün, K. Unger, *Colloids Surf. A* **2001**, *187–188*, 109–116.
[25] W. C. Davies, C. Morris, *J. Chem. Soc.* **1932**, 2880–2883.
[26] K. Saitoh, K. Ohashi, T. Oyama, A. Takahashi, J. Kadota, H. Hirano, K. Hasegawa, *J. Appl. Polym. Sci.* **2011**, *122*, 666–675.
[27] a) National Center for Biotechnology Information, PubChem Compound Summary for CID 11776, Triphenylphosphine., can be found under https://pubchem.ncbi.nlm.nih.gov/compound/Triphenylphosphine. (Accessed: 12.05.2021); b) National Center for Biotechnology Information, PubChem Compound Summary for CID 70071, Tris(4-methoxyphenyl) phosphine, can be found under https://pubchem.ncbi.nlm.nih.gov/compound/Tris_4-methoxyphenyl_phosphine. (Accessed: 12.05.2021).
[28] C. Bannwarth, S. Ehlert, S. Grimme, *J. Chem. Theory Comput.* **2019**, *15*, 1652–1671.
[29] a) TURBOMOLE V7.2 2017, a development of University of Karlsruhe and Forschungszentrum Karlsruhe GmbH, 1989–2007, TURBOMOLE GmbH, since 2007, can be found under http://www.turbomole.com. (Accessed: 27.05.2020); b) S. Metz, J. Kästner, A. A. Sokol, T. W. Keal, P. Sherwood, *Wiley Interdiscip. Rev.: Comput. Mol. Sci.* **2014**, *4*, 101–110; c) P. Sherwood, A. H. de Vries, M. F. Guest, G. Schreckenbach, C. A. Catlow, S. A. French, A. A. Sokol, S. T. Bromley, W. Thiel, A. J. Turner et al., *J. Mol. Struct.* **2003**, *632*, 1–28; d) J. Kästner, J. M. Carr, T. W. Keal, W. Thiel, A. Wander, P. Sherwood, *J. Phys. Chem. A* **2009**, *113*, 11856–11865.
[30] a) P. J. Stephens, F. J. Devlin, C. S. Ashvar, C. F. Chabalowski, M. J. Frisch, *Faraday Discuss.* **1994**, 103–119; b) S. Grimme, J. Antony, S. Ehrlich, H. Krieg, *J. Chem. Phys.* **2010**, *132*, p. 154104; c) F. Weigend, R. Ahlrichs, *Phys. Chem. Chem. Phys.* **2005**, *7*, 3297–3305.
[31] W. Humphrey, A. Dalke, K. Schulten, *J. Mol. Graphics* **1996**, *14*, 33–38.
[32] a) J. Parmentier, S. Saadhallah, M. Reda, P. Gibot, M. Roux, L. Vidal, C. Vix-Guterl, J. Patarin, *J. Phys. Chem. Solids* **2004**, *65*, 139–146; b) R. Ryoo, S. H. Joo, S. Jun, *J. Phys. Chem. B* **1999**, *103*, 7743–7746.
[33] D. Massiot, F. Fayon, M. Capron, I. King, S. Le Calvé, B. Alonso, J.-O. Durand, B. Bujoli, Z. Gan, G. Hoatson, *Magn. Reson. Chem.* **2002**, *40*, 70–76.

Manuscript received: June 11, 2021
Accepted manuscript online: July 12, 2021
Version of record online: August 5, 2021

